Editors' Suggestion

Intrinsic Nonlinear Hall Effect and Gate-Switchable Berry Curvature Sliding in Twisted Bilayer Graphene

Meizhen Huang,[1,*] Zefei Wu,[1,*,†,§] Xu Zhang,[2,*] Xuemeng Feng,[1] Zishu Zhou,[1] Shi Wang,[1] Yong Chen,[1,3] Chun Cheng,[3] Kai Sun,[4] Zi Yang Meng,[2,‡] and Ning Wang[1,‖]

[1]*Department of Physics and Center for Quantum Materials, The Hong Kong University of Science and Technology, Hong Kong, China*
[2]*Department of Physics and HKU-UCAS Joint Institute of Theoretical and Computational Physics, The University of Hong Kong, Hong Kong, China*
[3]*Department of Materials Science and Engineering, Southern University of Science and Technology, Shenzhen, China*
[4]*Department of Physics, University of Michigan, Ann Arbor, Michigan 48109, USA*

(Received 23 December 2022; revised 14 April 2023; accepted 26 June 2023; published 11 August 2023)

Though the observation of the quantum anomalous Hall effect and nonlocal transport response reveals nontrivial band topology governed by the Berry curvature in twisted bilayer graphene, some recent works reported nonlinear Hall signals in graphene superlattices that are caused by the extrinsic disorder scattering rather than the intrinsic Berry curvature dipole moment. In this Letter, we report a Berry curvature dipole induced intrinsic nonlinear Hall effect in high-quality twisted bilayer graphene devices. We also find that the application of the displacement field substantially changes the direction and amplitude of the nonlinear Hall voltages, as a result of a field-induced sliding of the Berry curvature hotspots. Our Letter not only proves that the Berry curvature dipole could play a dominant role in generating the intrinsic nonlinear Hall signal in graphene superlattices with low disorder densities, but also demonstrates twisted bilayer graphene to be a sensitive and fine-tunable platform for second harmonic generation and rectification.

DOI: 10.1103/PhysRevLett.131.066301

Introduction.—In the past few years, moiré superlattices, formed by stacking two layers of two-dimensional materials with a small twist angle, have led to many intriguing discoveries [1,2]. For example, unconventional superconductivity and correlated insulating states have been observed in flatbands of twisted bilayer graphene (TBG) [3–5], which offers a promising new platform to study strongly correlated many-body phenomena. In addition to correlation effects, moiré bands are also believed to offer nontrivial band topology [6–8], which is supported by the observation of ferromagnetism and quantum anomalous Hall effect in TBG aligned with BN, where the single spin- and valley-resolved miniband has a nontrivial Chern number [9–11], and nonlocal resistance in superlattice gaps of TBG originated from two nontrivial bulk Z_2 invariants [12]. While previous studies mostly focus on the global (or topological) properties of electronic wave functions, our knowledge about the k-space distribution of the Berry curvature remains limited. Studying Berry curvature properties within flatbands is of particular interest because it plays an important role not only in generating topological transport, but also in stabilizing correlated insulating states [13] and determing superfluid stiffness [14].

The nonlinear Hall effect (NHE) is the generation of a second harmonic Hall voltage in response to the injection current under time-reversal symmetric conditions [15]. Previous observations of NHE in low symmetry crystals [16,17], strained two-dimensional materials [18,19], and twisted transition metal dichalcoginides [20] have attracted great interest because of the potential applications, including frequency doubling and rectification [21,22]. Theoretical studies have shown that the NHE mainly has two possible microscopic origins. First, it can arise from a nonuniform distribution of the Berry curvature, also known as the Berry curvature dipole [15,23,24], and therefore becomes a powerful method to detect Berry curvatures in nonmagnetic quantum materials. Second, it can also arise from skew scattering [25,26], where the inherent chirality of the electron wave function induces transverse asymmetric scattering, which applies to a wider class of materials even without a Berry curvature dipole. In analogy to the intrinsic spin Hall effect which is caused by spin-orbit coupling in the band structure and survives in the limit of zero disorder, and the extrinsic spin Hall effect which is caused by spin-orbit coupling between Bloch electrons and impurities, here we call the Berry curvature dipole induced NHE as the intrinsic NHE, and the disorder-induced NHE as the extrinsic NHE. In graphene superlattices, the extrinsic NHE has been observed in graphene-BN superlattices and TBG [27,28], and intrinsic NHE has been recently observed in twisted double-bilayer graphene (TDBG) in the vicinity of the band gaps [29]. The former two works failed to observe any Berry curvature dipole behavior and the following one mainly focused on the gap properties instead of the flatband properties as Berry curvatures in TDBG predominantly reside in the vicinity of the band edges. Until now, whether

the Berry curvature or the scattering would play a dominant role in graphene superlattices was an open question. A systematic study of the Berry curvature dipole induced NHE inside the flatbands is still missing.

Here we studied the NHE inside the flatbands of TBG with a twist angle of 1.3°. By using this angle away from the magic angle, the strong correlation effect declines while band dispersion in TBG keeps relatively flat. The distribution of Berry curvature is diffused in the band and there will be significant signal from Berry curvature dipole detected within band, which distinguishes with the nonlinear Hall in TDBG, where the Berry curvatures are mostly accumulated nearly full fillings. Upon injecting an ac current, a second harmonic Hall voltage that scales quadratically with the injection current together with a vanishing second harmonic longitudinal response is observed, demonstrating a robust NHE originated from Berry curvature dipole. Even if the first harmonic transport properties of our TBG samples remain relatively unchanged upon the applied displacement field [2,30], we find that displacement field can slide the Berry curvature hotspots and lead to significant changes in the direction and amplitude of the nonlinear Hall signal. Our theoretical calculation fully explains the experimental observation of such electrically tunable NHE and reveals its origin from the sliding of the Berry curvature hotspots on the flatbands of the moiré superlattice. Our observation therefore establishes TBG as a fine-tunable platform for applications in second harmonic generation and rectification.

Experimental results.—TBG heterostructures, as schematically shown in Fig. 1(a), are fabricated by the "tear-and-stack" method [31]. A dual gate geometry is used to independently control the total carrier density n and the displacement field D (see Supplemental Material note 1 for details [32]). The scheme of longitudinal and transverse measurement is illustrated in Fig. 1(b). We first characterize the TBG device by measuring the longitudinal resistance R_{xx} and the Hall carrier density n_H as a function of the gate voltage (or, equivalently, the filling factor υ of the bands) at a temperature of $T = 1.5$ K. The sharp peak of R_{xx} near the charge neutral point (CNP) indicates the mobility $\sim$110 000 cm^2 V^{-1} s^{-1}. In TBG, single-particle gaps form at CNP and at a superlattice density of $n = \pm n_s = \pm 4/A$, where A is the moiré unit cell area and the factor 4 accounts for the spin and valley degeneracies. These fillings with single-particle gaps ($\upsilon = 0$ and ± 4) can be identified in Fig. 1(c) (vertical dashed lines) by peaks of R_{xx} and the sharp sign change in n_H, indicating the switching between electronlike to holelike pockets as the Fermi energy swap through a band gap. While additional R_{xx} peaks can be observed near the half filling and the quarter filling, n_H at these positions shows no anomalies and follows $n_H = n$, suggesting that the correlation effect is relatively small in this device and a Bistritzer-MacDonald type of the flatband model [2], which we adapt in the theoretical calculation of NHE below, offers a good description of such a system.

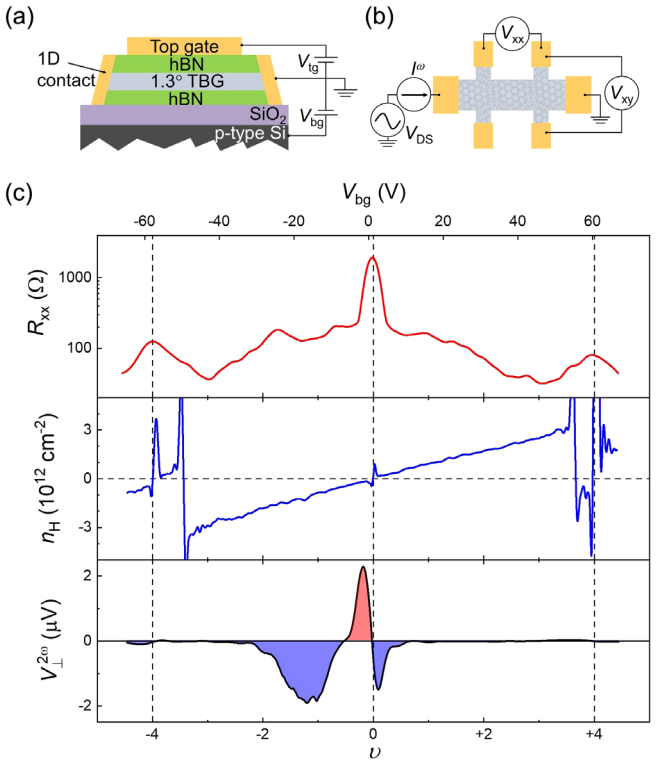

FIG. 1. Basic characterization of the TBG device. (a) Schematic structure of the 1.30° TBG device. The carrier density n and the displacement field D are controlled by the top and bottom gates with gate voltage V_{tg} and V_{bg}, respectively. (b) The four-probe measurement scheme. Here, we measure the longitudinal voltage V_{xx} and Hall voltage V_{xy} in the presence of an ac longitudinal current I^ω. (c) The longitudinal resistance $R_{xx} = V_{xx}/I^\omega$ (upper panel) and the carrier density measured via the Hall effect n_H (middle panel) as functions of υ and V_{bg} ($V_{tg} = 0$ V). The vertical dashed lines denote the CNP and fully filled moiré bands. Bottom panel: The second harmonic Hall voltage $V_\perp^{2\omega}$ as a function of filling factor υ measured at $I^\omega = 100$ nA and $T = 1.5$ K.

This behavior is also consistent with the observation of additional sign changes in n_H at $3 < |\upsilon| < 4$ that matches the electron-hole charge carrier switching point (or van Hove singularities) in the single-particle band structure [39,40]. From the superlattice density $n_s = 4 \times 10^{12}$ cm^{-2}, the twist angle of this device is determined to be 1.3°. It is worthwhile to highlight that by utilizing this twisting angle away from the magic angle, complicated many-body effects, such as the anomalous enhancement of the nonlinear Hall signal from divergent effective mass [20], are avoided so that a clean platform where semiclassical description for NHE from band anomalous velocity can be used is obtained to study the Berry curvature dipole of intrinsic band structures. The advantage of such a flatband is that the distribution of Berry curvature is diffused in band so that there will be significant signal from Berry curvature dipole detected within band.

It is important to note that an ideal TBG is not expected to exhibit NHE due to the threefold rotational symmetry,

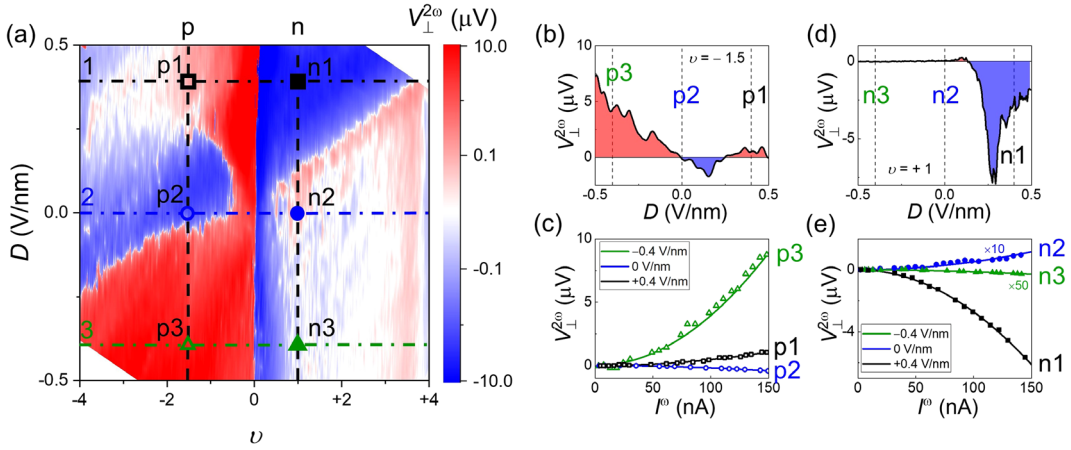

FIG. 2. Electric field tunable nonlinear Hall effect. (a) Filling and displacement field mapping of $V_\perp^{2\omega}$ measured at $T = 1.5$ K. Dashed lines marked with p and n indicate $\upsilon = -1.5$ and $\upsilon = +1$, respectively. Dash dotted lines marked with 1, 2, and 3 indicate three different fields: $D = +0.4, 0, -0.4$ V/nm. Their intersection points are named as shown in the figure. (b) $V_\perp^{2\omega}$ versus D measured at $\upsilon = -1.5$ at $I^\omega = 100$ nA. (c) $V_\perp^{2\omega}$ versus I^ω at various displacement fields at $\upsilon = -1.5$. Dots are the experimental data and the solid lines are parabolic fittings. (d),(e) Same as (b) and (c) for $\upsilon = +1$.

which forces the Berry curvature dipole (Λ) to be zero [15]. However, the strain that arises in the sample fabrication process can break this symmetry and induce a nonzero nonlinear Hall signal [41,42]. As shown in the bottom panel of Fig. 1(c), where the second harmonic Hall voltage $V_\perp^{2\omega}$ at $I^\omega = 100$ nA versus υ is plotted, nonzero responses are indeed observed. First of all, in agreement with the sign changes of Λ at band gaps [42,43], $V_\perp^{2\omega}$ changes signs at CNP and full fillings. In addition, $V_\perp^{2\omega}$ show two peaks with opposite signs near the band gaps, which can be understood by the Berry curvature hotspots near the edges of the gap. To verify that $V_\perp^{2\omega}$ is indeed from Berry curvature contributions instead of extrinsic effects such as defect scattering, additional experiment data is provided in Supplemental Material note 2 [32]. The filling, displacement field, and temperature dependent data can be captured by the calculated Berry curvature dipole, but cannot be explained by the scattering-induced nonlinear Hall response.

We then systematically study the dependence of NHE with an out-of-plane electric displacement field D which induces charge and voltage differences between the layers (D field dependence of the first harmonic transport data shown in Supplemental Material note 3 indicate that the effect of displacement field on first harmonic transport of TBG is very weak and disorder's contribution to transport is very small [32].). Figure 2(a) shows the map of $V_\perp^{2\omega}$ in the space of filling factor-displacement field (υ-D). $V_\perp^{2\omega}$ at $\upsilon = -1.5$ and at $\upsilon = +1$ are marked by the dashed line labeled with p and n in Fig. 2(a), respectively. The magnitude and direction of $V_\perp^{2\omega}$ changes when we tune D while keeping υ unchanged. To be more specific, $V_\perp^{2\omega}$ at $\upsilon = -1.5$ at various D is plotted in Fig. 2(b). A region with small negative values of $V_\perp^{2\omega}$ is observed between two positive $V_\perp^{2\omega}$ peaks. Moreover, $V_\perp^{2\omega}$ shows a clear quadratic current-voltage ($I - V$) characteristic for all D [Fig. 2(c)], which, combined with the 2ω frequency, indicates a robust nonlinear Hall effect. Similar D switchable $V_\perp^{2\omega}$ is observed in the conduction band [Figs. 2(d)–2(e)]. In addition, D switchable $V_\perp^{2\omega}$ is observed in other devices with different twist angles, as shown in Supplemental Material, Fig. 1. These observations show that D can effectively modulate the low-energy bands as well as the sign and the amplitude of the Berry curvature dipole Λ.

Berry curvature sliding induced switchable dipole.— Numerical studies are performed to study the origin of the observed D field effect in the observed NHE results in TBG. Band structure of TBG under a uniaxial strain is calculated by using the Bistritzer-MacDonald model with a strain strength of 0.3% (the electric field is introduced by considering an electrostatic energy difference between two layers). Berry curvature Ω is calculated using the numerical method proposed in Ref. [44]. The Λ can be determined using $\Lambda = \int_k (\partial f_0/\partial E)(\partial E/\partial k)\Omega$, where $\int_k = \mathrm{d}^2k/(2\pi)^2$, and f_0 is the fermion occupation number. In Fig. 3(a), the calculated Λ as functions of D and υ is plotted (disorder induced extrinsic NHE is not included in this calculation and discussed separately in Supplemental Material, notes 2 and 5 [32]). For a fixed υ, the calculated Λ shows an opposite sign for small D and large D, closely resembles the experimentally measured $V_\perp^{2\omega}$. In addition, experimental data shown in Fig. 1(c) can be captured by the theoretical calculation (see Supplemental Material, Fig. 5 [32]). These consistencies verify that the observed electrically tunable NHE indeed results from D field tunable Λ.

To understand the microscopic origin, results of band structure and Ω of strained TBG at three different D are shown in Fig. 3(b). As shown by our calculation and the experimental observations, in the accessible range of D,

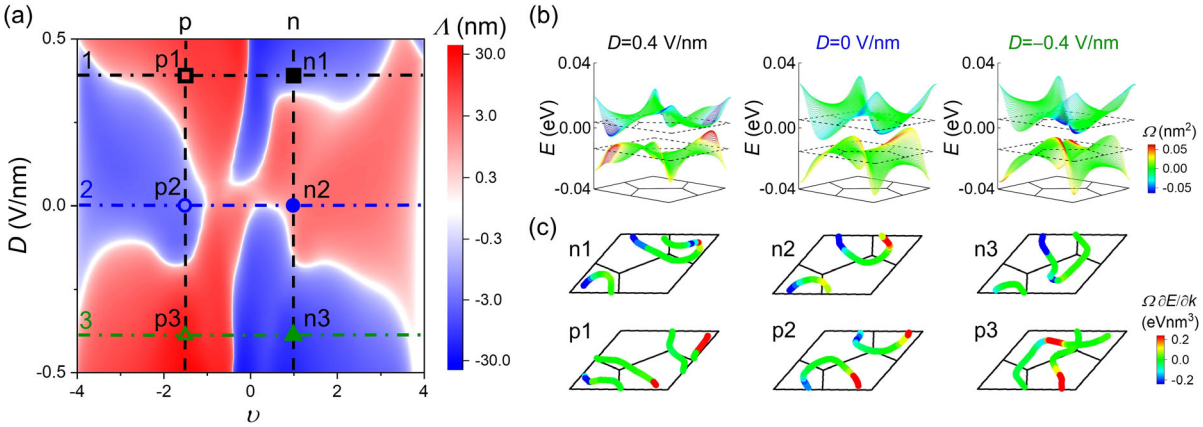

FIG. 3. Sliding of the Berry curvature hotspot. (a) Λ as a function of υ and D calculated by using the Bistritzer-MacDonald model with a strain strength of 0.3%. (b) Calculated band structure of the moiré bands near charge neutrality with $D = +0.4$, 0, and -0.4 V/nm. The color represents the value of Ω. The parallelogram marks the reciprocal lattice (high symmetry points are labeled in Supplemental Material, Fig. 9). (c) The distribution of the product of the Berry curvature Ω and the slope of the band distribution $(\partial E/\partial k)$ within the reciprocal lattice at the energies marked by the dashed parallelograms in (b) at six representative points in (a). The zero-temperature dipole moment can be calculated by integrating $\Omega(\partial E/\partial k)$ at the Fermi level in the first moiré Brillouin zone.

single-particle gaps at CNP continuously present due to the breaking inversion symmetry in strained TBG. There is no band close-reopen happening which may change the sign of Ω. Instead, when tuning D, the location of the Ω hotspot (indicated by the blue and red region) moves due to the change in the band structure. In Fig. 3(c), the distribution of $\Omega(\partial E/\partial k)$ inside the reciprocal lattice at six representative points are plotted. The Λ can then be determined using $\Lambda = \int_k (\partial f_0/\partial E)(\partial E/\partial k)\Omega$. For $\upsilon = +1$ at $D = +0.4$ (point n1) and -0.4 V/nm (point n3), the dominated negative values of $\Omega(\partial E/\partial k)$ in the reciprocal lattice lead to a negative Λ. When D is between these two values, at point n2, the location of the Ω hotspot slides into a band region that has a different sign of the band dispersion $(\partial\varepsilon/\partial k)$, leading to a sign change of $\Omega(\partial E/\partial k)$. Similarly, for the valence band (labeled with p1, p2 and p3), the predominantly values of $\Omega(\partial E/\partial k)$ at p1 and p3 is positive, and the sliding leads to negative values of $\Omega(\partial E/\partial k)$ at p2. Since $\Lambda = \int_k (\partial f_0/\partial E)(\partial E/\partial k)\Omega$, it is understandable that the sliding of Ω hotspot on band structure can induce sign changes of Λ.

Discussion.—To this end, we would like to comment on the two types of NHEs. It is proposed that both the Berry curvature dipole and the disorder scattering could induce a nonlinear Hall signal. The dipole contribution depends on the strain strength, and the disorder contribution depends on the disorder density. In TBG, according to theoretical calculation [45], an exponential decay form factor $\lambda(k, k + q + Q)$ with momentum transfer "$q + Q$" kills large momentum scattering tails out of several moiré Brillouin zones. Local disorder with carbon atom size has long momentum tail scaling as graphene Brillouin zone after Fourier transformation so that the form factor will sharply suppress the contribution from this kind of disorder (also the most common disorder). As a result, only spatially extended scatterer in moiré unit cell level (denoted as effective disorder) with small momentum scattering within the moiré Brillouin zone dominates in TBG's nonlinear transport. To compare the extrinsic (disorder) contribution with the intrinsic (dipole) contribution, Fig. 4 is provided, where screened charged Coulomb potential from effective disorder is used to compute the skew scattering contribution for NHE and detailed calculations can be found in Supplemental Material, note 5 [32]. The nonlinear signal is

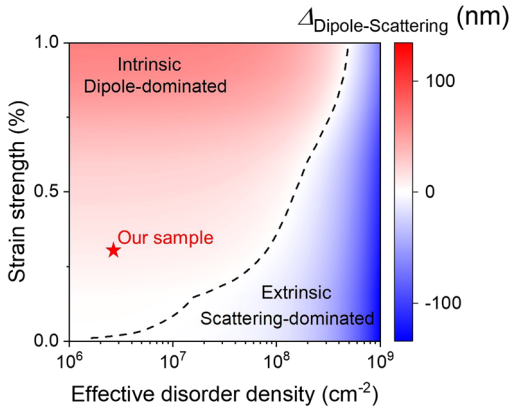

FIG. 4. Phase diagram of the NHE. The color marks the difference between the Berry curvature dipole and the effective dipole of the scattering mechanism $\Delta_{\text{Dipole}-\text{scattering}}$. The dashed line represents the position where the Berry curvature dipole and the scattering contribute equally to the nonlinear Hall signal. The red (blue) area represents the dipole (scattering) dominated area. The strain strength is the total uniaxial strain used in theoretical calculation. The effective disorder is from screened Coulomb potential scatterer.

dipole dominated at a relatively large strain and a small effective disorder density (which is the case in our sample marked by star in Fig. 4 with a high mobility $\sim 110\,000\ \mathrm{cm^2\,V^{-1}\,s^{-1}}$ and a effective disorder density $\sim 2.7 \times 10^6\ \mathrm{cm^{-2}}$), and scattering dominated at the opposite (observed in TBG with mobility $\sim 23\,000\ \mathrm{cm^2\,V^{-1}\,s^{-1}}$ and a disorder density $\sim 3.4 \times 10^8\ \mathrm{cm^{-2}}$ [27]). Since the disorder strength can hardly be controlled, it is much easier and simpler to control the nonlinear Hall signal in high-quality TBG devices by manipulating the intrinsic dipole contribution via tuning the strain strength using flexible substrates [19].

In summary, we observed electrically tunable intrinsic NHE in TBG. In contrast to recent studies about the scattering-induced second harmonic generation in graphene superlattice [27,28], the NHE in our devices is induced by a nonzero Berry curvature dipole. In addition, our study indicates that the Berry curvature distribution in TBG is highly sensitive to the out-of-plane displacement field, which offers a highly efficient way to control or vary the amplitude and direction of the Berry curvature dipole, and thus the NHE. Our theoretical model calculation, where the sliding of the Berry curvature hotspots due to the interplay of strain, displacement field and flatband structure, semiquantitatively explains the experimental results. This Letter not only elucidates the intrinsic origin of the NHE in high-quality TBG to be the Berry curvature distribution inside the flatbands but also highlights TBG to be a fine-tunable platform for second harmonic generation and rectification.

Grant support from the National Key R&D Program of China (2020YFA0309600) and the Research Grants Council (RGC) of Hong Kong (Project No. AoE/P701/20, 16303720, C6025-19G, and C7037-22G) are acknowledged. X. Z. and Z. Y. M. also acknowledge support from the RGC of Hong Kong (Project No. 17301420, No. 17301721, No. 17309822), the ANR/RGC Joint Research Scheme sponsored by RGC of Hong Kong and French National Research Agency (Project No. A_HKU703/22), the K. C. Wong Education Foundation (Grant No. GJTD-2020-01). Device fabrication was performed at the MCPF and WMINST of HKUST with great technical support from Mr. LAI Chun Kit and Dr. Yuan Cai.

Z.-F. W. and M.-Z. H. conceived the project and designed the experiments. M.-Z. H. and Z.-F. W. fabricated the devices, performed the measurements, analyzed the data, and wrote the manuscript. Z. Y. M., K. S., and X. Z. performed theoretical computations and polished the manuscript. X.-M. F., Z.-S. Z., S. W., Y. C., and C. C. provided technical support in the device fabrication process. N. W. finalized the manuscript with contributions from all authors.

[*] These authors contributed equally to this work.
[†] Corresponding author.
zefei.wu@manchester.ac.uk
[‡] Corresponding author.
zymeng@hku.hk
[‖] Corresponding author.
phwang@ust.hk
[§] Present address: Department of Physics and Astronomy and National Graphene Institute, University of Manchester, Manchester M13 9PL, United Kingdom.

[1] E. Y. Andrei and A. H. MacDonald, Nat. Mater. **19**, 1265 (2020).
[2] R. Bistritzer and A. H. MacDonald, Proc. Natl. Acad. Sci. U.S.A. **108**, 12233 (2011).
[3] Y. Cao, V. Fatemi, A. Demir, S. Fang, S. L. Tomarken, J. Y. Luo, J. D. Sanchez-Yamagishi, K. Watanabe, T. Taniguchi, E. Kaxiras, R. C. Ashoori, and P. Jarillo-Herrero, Nature (London) **556**, 80 (2018).
[4] Y. Cao, V. Fatemi, S. Fang, K. Watanabe, T. Taniguchi, E. Kaxiras, and P. Jarillo-Herrero, Nature (London) **556**, 43 (2018).
[5] M. Yankowitz, S. Chen, H. Polshyn, Y. Zhang, K. Watanabe, T. Taniguchi, D. Graf, F. Young Andrea, and R. Dean Cory, Science **363**, 1059 (2019).
[6] N. Bultinck, S. Chatterjee, and M. P. Zaletel, Phys. Rev. Lett. **124**, 166601 (2020).
[7] J. Liu and X. Dai, Phys. Rev. B **103**, 035427 (2021).
[8] C. W. Song Justin, P. Samutpraphoot, and S. Levitov Leonid, Proc. Natl. Acad. Sci. U.S.A. **112**, 10879 (2015).
[9] M. Serlin, C. L. Tschirhart, H. Polshyn, Y. Zhang, J. Zhu, K. Watanabe, T. Taniguchi, L. Balents, and A. F. Young, Science **367**, 900 (2020).
[10] L. Sharpe Aaron, J. Fox Eli, W. Barnard Arthur, J. Finney, K. Watanabe, T. Taniguchi, M. A. Kastner, and D. Goldhaber-Gordon, Science **365**, 605 (2019).
[11] G. Chen, A. L. Sharpe, E. J. Fox, Y.-H. Zhang, S. Wang, L. Jiang, B. Lyu, H. Li, K. Watanabe, T. Taniguchi, Z. Shi, T. Senthil, D. Goldhaber-Gordon, Y. Zhang, and F. Wang, Nature (London) **579**, 56 (2020).
[12] C. Ma, Q. Wang, S. Mills, X. Chen, B. Deng, S. Yuan, C. Li, K. Watanabe, T. Taniguchi, X. Du, F. Zhang, and F. Xia, Nano Lett. **20**, 6076 (2020).
[13] Y. Xie, A. T. Pierce, J. M. Park, D. E. Parker, E. Khalaf, P. Ledwith, Y. Cao, S. H. Lee, S. Chen, P. R. Forrester, K. Watanabe, T. Taniguchi, A. Vishwanath, P. Jarillo-Herrero, and A. Yacoby, Nature (London) **600**, 439 (2021).
[14] H. Tian, X. Gao, Y. Zhang, S. Che, T. Xu, P. Cheung, K. Watanabe, T. Taniguchi, M. Randeria, F. Zhang, C. N. Lau, and M. W. Bockrath, Nature (London) **614**, 440 (2023).
[15] I. Sodemann and L. Fu, Phys. Rev. Lett. **115**, 216806 (2015).
[16] Q. Ma *et al.*, Nature (London) **565**, 337 (2019).
[17] K. Kang, T. Li, E. Sohn, J. Shan, and K. F. Mak, Nat. Mater. **18**, 324 (2019).
[18] S.-C. Ho, C.-H. Chang, Y.-C. Hsieh, S.-T. Lo, B. Huang, T.-H.-Y. Vu, C. Ortix, and T.-M. Chen, National electronics review **4**, 116 (2021).
[19] J. Son, K.-H. Kim, Y. H. Ahn, H.-W. Lee, and J. Lee, Phys. Rev. Lett. **123**, 036806 (2019).

[20] M. Huang, Z. Wu, J. Hu, X. Cai, E. Li, L. An, X. Feng, Z. Ye, N. Lin, K. T. Law, and N. Wang, Natl. Sci. Rev. **10**, nwac232 (2023).
[21] H. Isobe, S. Y. Xu, and L. Fu, Sci. Adv. **6**, eaay2497 (2020).
[22] Y. Zhang and L. Fu, Proc. Natl. Acad. Sci. U.S.A. **118**, e2100736118 (2021).
[23] Z. Z. Du, H.-Z. Lu, and X. C. Xie, Nat. Rev. Phys. **3**, 744 (2021).
[24] Z. Z. Du, C. M. Wang, H.-Z. Lu, and X. C. Xie, Phys. Rev. Lett. **121**, 266601 (2018).
[25] Z. Z. Du, C. M. Wang, S. Li, H.-Z. Lu, and X. C. Xie, Nat. Commun. **10**, 3047 (2019).
[26] Z. Z. Du, C. M. Wang, H.-P. Sun, H.-Z. Lu, and X. C. Xie, Nat. Commun. **12**, 5038 (2021).
[27] J. Duan, Y. Jian, Y. Gao, H. Peng, J. Zhong, Q. Feng, J. Mao, and Y. Yao, Phys. Rev. Lett. **129**, 186801 (2022).
[28] P. He, G. K. W. Koon, H. Isobe, J. Y. Tan, J. Hu, A. H. C. Neto, L. Fu, and H. Yang, Nat. Nanotechnol. **17**, 378 (2022).
[29] S. Sinha, P. C. Adak, A. Chakraborty, K. Das, K. Debnath, L. D. V. Sangani, K. Watanabe, T. Taniguchi, U. V. Waghmare, A. Agarwal, and M. M. Deshmukh, Nat. Phys. **18**, 765 (2022).
[30] K. Kim, A. DaSilva, S. Huang, B. Fallahazad, S. Larentis, T. Taniguchi, K. Watanabe, J. LeRoy Brian, H. MacDonald Allan, and E. Tutuc, Proc. Natl. Acad. Sci. U.S.A. **114**, 3364 (2017).
[31] K. Kim, M. Yankowitz, B. Fallahazad, S. Kang, H. C. P. Movva, S. Huang, S. Larentis, C. M. Corbet, T. Taniguchi, K. Watanabe, S. K. Banerjee, B. J. LeRoy, and E. Tutuc, Nano Lett. **16**, 1989 (2016).
[32] See Supplemental Material at http://link.aps.org/supplemental/10.1103/PhysRevLett.131.066301 for further experimental data and computational details, which includes Refs. [33–38].
[33] L. Wang, I. Meric, P. Y. Huang, Q. Gao, Y. Gao, H. Tran, T. Taniguchi, K. Watanabe, L. M. Campos, D. A. Muller, J. Guo, P. Kim, J. Hone, K. L. Shepard, and C. R. Dean, Science **342**, 614 (2013).
[34] Z. Bi, N. F. Q. Yuan, and L. Fu, Phys. Rev. B **100**, 035448 (2019).
[35] N. N. T. Nam and M. Koshino, Phys. Rev. B **96**, 075311 (2017).
[36] K. Uchida, S. Furuya, J.-I. Iwata, and A. Oshiyama, Phys. Rev. B **90**, 155451 (2014).
[37] H. Kim, N. Leconte, B. L. Chittari, K. Watanabe, T. Taniguchi, A. H. MacDonald, J. Jung, and S. Jung, Nano Lett. **18**, 7732 (2018).
[38] A. V. Maharaj, I. Esterlis, Y. Zhang, B. J. Ramshaw, and S. A. Kivelson, Phys. Rev. B **96**, 045132 (2017).
[39] S. Chen, M. He, Y.-H. Zhang, V. Hsieh, Z. Fei, K. Watanabe, T. Taniguchi, D. H. Cobden, X. Xu, C. R. Dean, and M. Yankowitz, Nat. Phys. **17**, 374 (2021).
[40] S. Wu, Z. Zhang, K. Watanabe, T. Taniguchi, and E. Y. Andrei, Nat. Mater. **20**, 488 (2021).
[41] A. Kerelsky, L. J. McGilly, D. M. Kennes, L. Xian, M. Yankowitz, S. Chen, K. Watanabe, T. Taniguchi, J. Hone, C. Dean, A. Rubio, and A. N. Pasupathy, Nature (London) **572**, 95 (2019).
[42] P. A. Pantaleón, T. Low, and F. Guinea, Phys. Rev. B **103**, 205403 (2021).
[43] C.-P. Zhang, J. Xiao, B. T. Zhou, J.-X. Hu, Y.-M. Xie, B. H. Yan, and K. T. Law, Phys. Rev. B **106**, L041111 (2022).
[44] T. Fukui, Y. Hatsugai, and H. Suzuki, J. Phys. Soc. Jpn. **74**, 1674 (2005).
[45] B. A. Bernevig, Z.-D. Song, N. Regnault, and B. Lian, Phys. Rev. B **103**, 205411 (2021).